Meshfree Modeling and Analysis of Physical Fields in Heterogeneous Media

I.Tsukanov, V.Shapiro*
Spatial Automation Laboratory
University of Wisconsin-Madison
1513 University Avenue
Madison, WI, 53706-1572, USA

March 10, 2004

Abstract

Continuous and discrete variations in material properties lead to substantial difficulties for most mesh-based methods for modeling and analysis of physical fields. The meshfree method described in this paper relies on distance fields to boundaries and to material features in order to represent variations of material properties as well as to satisfy prescribed boundary conditions. The method is theoretically complete in the sense that all distributions of physical properties and all physical fields are represented by generalized Taylor series expansions in terms of powers of distance fields. We explain how such Taylor series can be used to construct *solution structures* – spaces of functions satisfying the prescribed boundary conditions exactly and containing the necessary degrees of freedom to satisfy additional constraints. Fully implemented numerical examples illustrate the effectiveness of the proposed approach.

Keywords: heterogeneous material, distance field, meshfree method, boundary condition

1 Introduction

1.1 Challenges in modeling physical fields in heterogeneous media

Variation of the physical properties of heterogeneous media substantially complicates the modeling of physical fields on a computer. The "standard" mathematical models derived for homogeneous media do not correctly describe the physical processes in media with spatially varying physical properties. Modeling of physical fields in heterogeneous media has to deal with a number of special cases of heterogeneity. Such special cases include continuous and discrete (discontinuous) changes of the media physical properties. Discrete changes of the properties occur on the interface boundaries between materials with distinct physical properties. This type of heterogeneity takes place quite often, and it requires introduction of interface boundary conditions on the boundary of a contact. The mathematical formulation of such boundary conditions depends on the physical process being modeled. For example, in the case of heat transfer, the interface boundary conditions require equality of temperature and heat fluxes through the boundary of a contact; in stress analysis problems, interface boundary conditions can be formulated as continuous deformations along the boundary of a contact. Interface boundary conditions in most situations cause discontinuities in the normal derivatives of the solution along the interface boundary.

Continuous variations of physical properties require more significant changes in the mathematical formulation of the physical problem. For example, the general equation of heat transfer

$$div\,(\lambda \nabla u) = c\rho \frac{\partial u}{\partial t} - q_v \tag{1}$$

*Corresponding author. E-mail addresses: vshapiro@engr.wisc.edu, tsukanov@engr.wisc.edu

in the case of heterogeneous media with continuously varied thermal conductivity $\lambda = \lambda(p)$, specific heat $c = c(p)$ and specific weight $\rho = \rho(p)$ becomes

$$\lambda(p)\nabla^2 u + \nabla\lambda(p)\nabla u = c(p)\rho(p)\frac{\partial u}{\partial t} - q_v, \tag{2}$$

where $p(\mathbf{x})$ is a point in space. Equation (2) differs from the differential equation describing heat transfer in homogeneous media by the term $\nabla\lambda(p)\nabla u$. Simple examination of equation (2) suggests that this term might be significant and it cannot be ignored if the heterogeneous medium possesses considerable gradient in thermal conductivity. In this paper, we will focus on steady heat transfer in heterogeneous media, without distributed heat sources inside the domain. With these assumption equation (2) simplifies to

$$\lambda(p)\nabla^2 u + \nabla\lambda(p)\nabla u = 0. \tag{3}$$

Variation of physical properties also creates additional challenges for numerical methods used for computer simulation of physical processes. Most traditional analysis methods employ a spatial mesh that approximates the geometric model. It is also used to prescribe boundary conditions, to construct basis functions with good approximation properties and to perform integration. For heterogeneous media, the mesh also must take into account the variation of physical properties as well: the mesh should be denser in the regions with rapid variation of material properties, and it should match discontinuities at the interfaces. This further complicates the meshing process, and the overall solution procedures.

Difficulties in meshing, lack of standard computer representations for heterogeneous media, and built-in mathematical models that do not account for variation of physical properties have prevented support for heterogeneous materials by standard CAD systems.

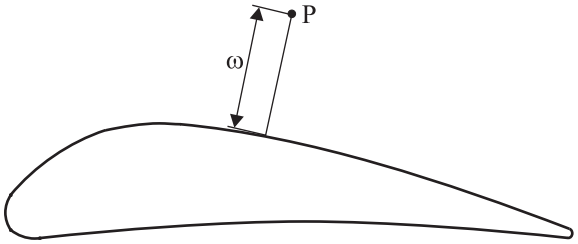

Figure 1: Airfoil contour

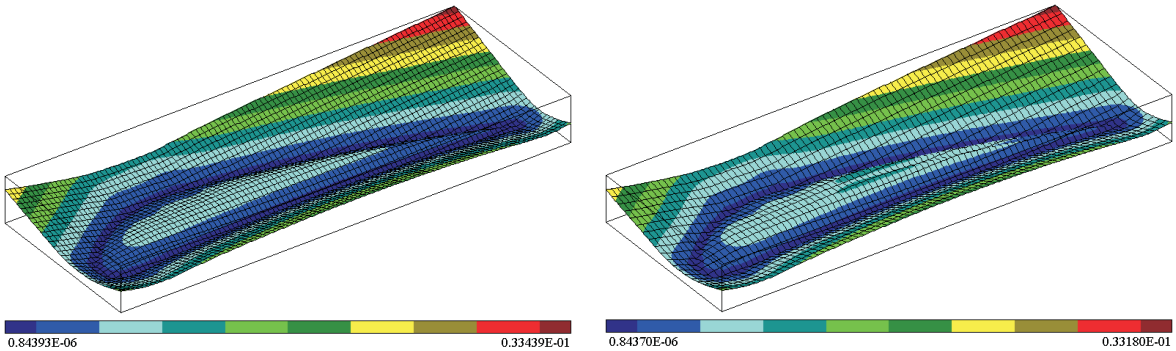

(a) (b)

Figure 2: Distance fields to the contour of the airfoil shown in Figure 1: (a) normalized to the first order and (b) normalized to the second order

1.2 Meshfree method with distance fields

In this paper we present a meshfree method that addresses most of the aforementioned challenges. The term *meshfree* implies that the method does not necessarily require a spatial discretization that conforms to the shape of the geometric domain. Instead, meshfree methods employ discretization in functional space. The salient feature of the method we describe here is exact treatment of all prescribed boundary conditions. This is possible because the method represents physical fields in terms of functions of distances to boundaries of a geometric object. Loss of differentiability at equidistant points prevents the use of the exact distance functions in engineering applications. However, this limitation can be overcome by replacing exact distances with various smooth approximations, while preserving most of the attractive properties of the distance fields. In particular, we can replace the exact distance fields with their m-th order approximations in the following sense, originally described by Rvachev [19]. Suppose point p is a point on the boundary of set Ω, and n is a unit vector pointing away from Ω towards some points that are closer to p than to any other point in Ω. In other words, n coincides with unit normal on smooth points of the boundary, but the notion of the normal direction is also well defined at sharp corners. A suitable m-th order approximation of the exact distance is a function ω that is obtained by requiring that only *some* of the higher order derivatives vanish, that is for all points p on the boundary of Ω:

$$\left.\frac{\partial \omega}{\partial n}\right|_{\partial\Omega} = 1; \qquad \left.\frac{\partial^k \omega}{\partial n^k}\right|_{\partial\Omega} = 0; \qquad k = 2, 3, \ldots, m. \tag{4}$$

Such a function ω is called *normalized*[1] to the m-th order. Normalized functions behave like the distance function near their zero set (corresponding to the boundary of set Ω) and tend to smoothly approximate the distance function away from $\partial\Omega$. However, normalization is a local property and cannot guarantee that the function behaves as the distance function away from the boundary points. Figure 2(a) shows an approximate distance field normalized to the first order for the airfoil profile (Figure 1). A higher order of normalization implies better approximation of the exact distance field, particularly near the boundary of Ω. For example, Figure 2(b) shows a plot of the distance field normalized to the second order.

Normalized approximate distance fields exist for virtually all geometric objects of interest in engineering [24] and can be constructed by a variety of methods. In particular, the theory of R-functions [23, 19] offers a systematic and algorithmic method for constructing such functions automatically for curves, surfaces, and solids. This method was used to construct the field in Figures 2(a) and 2(b), as well as the approximate distance fields shown in Figure 11. Additional details on R-functions and implemented techniques can be found in [25, 1].

The initial idea of the meshfree method we describe in this paper belongs to Kantorovich [13]. He proposed to represent functions satisfying Dirichlet boundary condition $u|_{\partial\Omega} = \varphi$ in the form:

$$u = \varphi + \omega\Phi, \tag{5}$$

where ω is a distance field to the boundary $\partial\Omega$, and Φ is an arbitrary function. Since ω takes on zero value on $\partial\Omega$, function u satisfies the prescribed Dirichlet boundary condition regardless of function Φ. Later, Rvachev noticed that expression (5) is a zero order Taylor series expansion of u by powers of the distance field ω with the product $\omega\Phi$ playing the role of a remainder term. Generalizing Kantorovich's idea, Rvachev showed that any function can be represented by power series of a distance field ω:

$$u = u_0^* + \sum_{i=1}^{m} u_i^* \frac{\omega^i}{i!} + \omega^{m+1}\Phi. \tag{6}$$

This power series looks very similar to classical Taylor series. In fact, if coefficients $\{u_i^*\}_{i=0}^m$ represent normal derivatives of u prescribed at the zero set of the distance field ω, the power series (6) represent a *generalized Taylor series* expansion of the function u by powers of the distance field ω. The major difference between the generalized and the classical Taylor series is the fact that the coefficients $\{u_i^*\}_{i=0}^m$ in the generalized Taylor series might be functions of spatial coordinates and/or distance field. However, in order to represent normal derivatives of u prescribed on the boundary $\partial\Omega$ these coefficients have to be constant up to mth order in the normal direction to the boundary. This implies that

$$\left.\frac{\partial^k u_i^*}{\partial n^k}\right|_{\partial\Omega} = 0, \qquad i = 1, \ldots, m. \tag{7}$$

[1] This terminology is consistent with the term *normal* function that is often used synonymously with the distance function.

Most of the functions prescribed as boundary conditions do not satisfy condition (7) automatically. In [19] Rvachev showed that if the distance field ω is normalized up to mth order, coordinate transformation $\mathbf{x} - \omega(\mathbf{x})\nabla\omega(\mathbf{x})$ applied to the function's arguments enforces the function to satisfy condition (7). We call the operation that transforms any function u into function satisfying the condition (7) *conditioning* of the function u. Conditioning via coordinate transformation is not always convenient. In such cases another way can be used to condition the function: $u^* = u - \sum_{i=1}^{m} \frac{1}{i!}\frac{\partial^i u}{\partial n^i}\omega^i$. Notice that the normal derivatives $\frac{\partial^i u}{\partial n^i}$, $i = 1, \ldots, m$ are defined only on the boundary of a geometric domain, but the last expression assumes their computation at any point of the domain. Rvachev showed that these normal derivatives can be extended by the differential operator

$$D_i^{\omega}() = (\nabla() \cdot \nabla\omega)^i \tag{8}$$

[19], therefore another means to condition a function appears as follows:

$$u^* = u - \sum_{i=1}^{m} \frac{1}{i!}\omega^i D_i^{\omega}(u). \tag{9}$$

The remainder term $\omega^{m+1}\Phi$ ensures the completeness of u [20], and it can be used to enforce additional constraints. For example, the remainder term can be chosen in such a way that u satisfies either a differential equation or minimizes a functional. Since in most cases it is impossible to determine function Φ exactly, it is usually approximated by linear combination of some basis functions:

$$\Phi = \sum_{i=1}^{N} C_i \chi_i. \tag{10}$$

Thus, a typical solution procedure aims to compute numerical values of the coefficients C_i that give the best approximation to the additional constraints. Rvachev and his students have developed this approach into Rvachev Functions Method (RFM) [2], and they applied it to solution of many physical problems.

1.3 Outline

In the remainder of this paper we apply the above meshfree method specifically to modeling material properties and physical fields in heterogeneous media.

Section 2 explains how the physical properties of heterogeneous media can be represented via the generalized Taylor series (6) and transfinite interpolation [21]. We will demonstrate how terms in the Taylor series control the distribution of the physical properties being modeled. Using a turbine blade model (inpired by [17]), we show how the remainder term in the Taylor series can be used to satisfy additional constraints on the distribution of the properties of a heterogeneous medium. The constructed heterogeneous models are used in Section 3, where the same meshfree method is used to formulate and solve the heat conduction problem while the generalized Taylor series (6) is used to satisfy the prescribed boundary conditions exactly. Section 3.3 deals with temperature fields in piecewise heterogeneous materials, for example such as arise in a titanium turbine blade coated with ceramics. We also explain the basic steps of the solution procedure, including construction of the basis functions and adaptive numerical integration over the unmeshed geometric model. Conclusions and future directions are summarized in Section 4.

2 Material properties as functions of distance fields

2.1 Completeness

Much of the existing literature on material modeling points in the direction of one natural parameter: the distance from a material feature. For design purposes, it is convenient and intuitive to specify how material composition changes as a function of the distance from the material feature. Capabilities of manufacturing processes for functionally-graded materials are also commonly described by their ability to modify material as functions of distance (determined either

[2] Originally, RFM stood for the "R-functions Method" because R-functions were one of the main tools for constructing approximate distance fields. However, the meshfree method with distance fields does not critically rely on R-functions and can be used with any smooth normalized approximations of distance fields.

analytically or experimentally) [16, 8]. The importance of distance modeling has already been recognized by other researchers. The most common types of material functions constructed by methods based on spatial discretization appear to be either the Euclidean distance function, weighted distance functions or simple functions of a distance function [3, 28, 27, 15, 10].

In [2] we propose to represent physical properties of heterogeneous media by functions of distance fields. Such functions can be constructed using generalized Taylor series expansion by powers of distance fields and inverse distance weighting transfinite interpolation [21]. This representation of material properties possesses several advantages. First of all, the use of generalized Taylor series and transfinite interpolation allows to satisfy the prescribed material conditions at specified geometric features exactly. Transfinite interpolation, described in [21], restricts neither the dimension nor the topology of geometric features and assures the analytic properties of the constructed functions. In [20] we proved completeness of the representation of functions via generalized Taylor series as follows:

Theorem 1 *Let Ω be a closed region; $f \in C^s(\Omega)$ be of $s > m$ times continuously differentiable function defined in the interior of Ω. Values of function f and its partial derivatives up to order m are prescribed on boundary $\partial\Omega$. Then for any small ε there exists a polynomial P_r such that inequality*

$$\|\gamma - \omega^{m+1} P_r\|_{H^s(\Omega)} < \varepsilon \tag{11}$$

is satisfied, where $\gamma = f - u$ is a function that vanishes on $\partial\Omega$ together with its partial derivatives up to order m.

The function u is constructed, for example, using the terms from the generalized Taylor series (6), in such a way that u coincides with function f and its partial derivatives up to order m on the boundary $\partial\Omega$. Then, Theorem 1 simply means that any and all functions can be represented by power series (6) of distance field ω. Reference [20] contains a proof of a general theorem regarding completeness in the presence of different boundary conditions on different portions of the boundary.

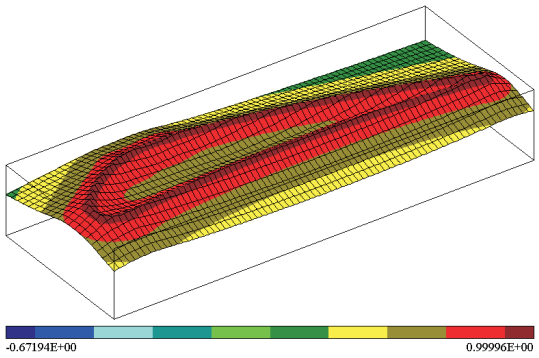

Figure 3: Plot of function $u = e^{-50\omega}$, where ω is a distance field to the airfoil boundary shown in Figure 1

2.2 Explicitly defined material functions

Similarly to the classical Taylor series, the generalized Taylor series requires computation of the derivatives of the function with respect to the distance field ω and their evaluation at $\omega = 0$:

$$u = u(0) + \sum_{i=1}^{m} \frac{1}{i!} \left. \frac{\partial^i u}{\partial \omega^i} \right|_{\omega=0} \omega^i + O\left(\omega^{m+1}\right) \tag{12}$$

For example, let expand a function $u = e^{-50\omega}$ into a power series by distance field ω. After computing and evaluating the derivatives of u at $\omega = 0$, we obtain the following power series that approximates function $u = e^{-50\omega}$:

$$u = 1 - 50\omega + 1250\omega^2 - \frac{62500}{3}\omega^3 + \frac{781250}{3}\omega^4 + O\left(\omega^5\right). \tag{13}$$

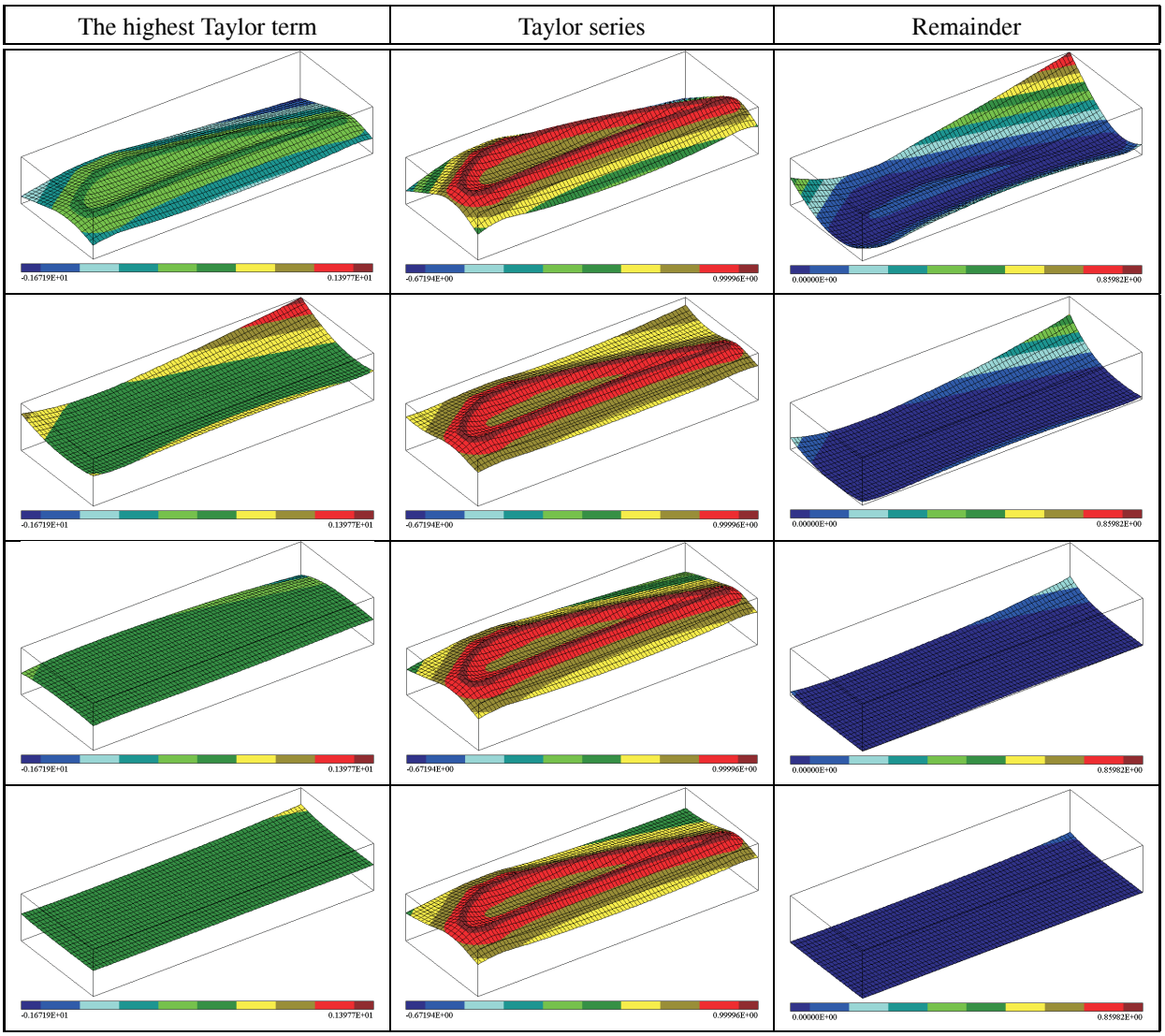

Table 1: Figures show decay of the remainder term in the Taylor series approximating the function $e^{-50\omega}$ with an increasing number of terms. The first column shows distributions of the highest term in the Taylor series (13): -50ω, $1250\omega^2$, $-\frac{62500}{3}\omega^3$, $\frac{781250}{3}\omega^4$. The second column presents partial sums of the Taylor series (13), and the third column shows distributions of the absolute value of the remainder term

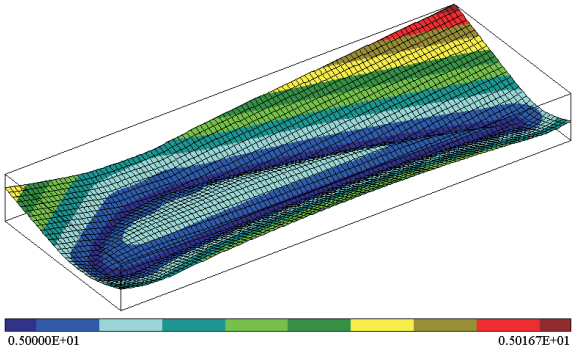

Figure 4: Plot of the function satisfying the conditions $u|_{\partial\Omega} = 5$; $\frac{\partial u}{\partial n}\big|_{\partial\Omega} = 0.5$

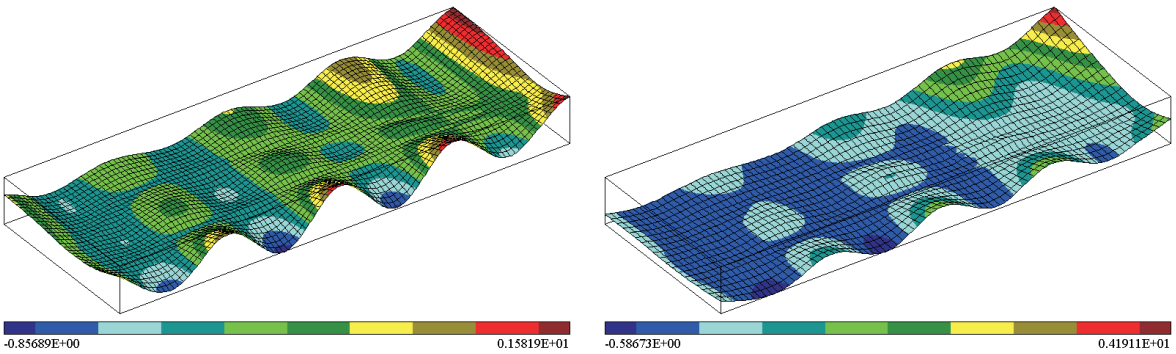

(a) (b)

Figure 5: (a) Plot of the function satisfying the conditions $u|_{\partial\Omega} = 10x^2$; $\frac{\partial u}{\partial n}\big|_{\partial\Omega} = 10 - 50(1 - 10y)\sin(100x)$. (b) Plot of the function satisfying the conditions $u|_{\partial\Omega} = 10x^2$; $\frac{\partial u}{\partial n}\big|_{\partial\Omega} = 10 - 50(1 - 10y)\sin(100x)$; $\frac{\partial^2 u}{\partial n^2}\Big|_{\partial\Omega} = 10^4 x$

The plots in the first column of Table 1 show the first four terms in the series (13), while the plots in the second column show the corresponding partial sums of the of the series; as the number of terms in the series increases, so does its accuracy of approximation of the function $u = e^{-50\omega}$. Plots shown in the third column of Table 1 show the absolute value of the remainder term in each case (computed as the difference between function $u = e^{-50\omega}$ and its partial Taylor series (13)).

Generalized Taylor series can be also used as a construction tool to create functions with desired analytical properties prescribed over geometric features. Below we consider several common cases. Up to the remainder term, the procedure is basically syntactic because it involves *no* numerical computations. Hence, in the rest of this Section and in Section 2.4, we will ignore the remainder term by setting function Φ to zero. We will explain the role of the remainder term in Section 2.4.

We start with the simplest special case where constant function's value and constant normal derivatives are prescribed over a geometric feature. Figure 4 shows the plot of the function taking on a value of 5 on the airfoil contour shown in Figure 1 with first normal derivative of $\frac{1}{2}$. Analytic expression for this function is very simple:

$$u = 5 + \frac{1}{2}\omega, \tag{14}$$

where ω is a distance field shown in Figure 2(a). It is easy to verify that the prescribed conditions are satisfied on the geometric feature. Indeed, since ω is zero on the airfoil contour $u|_{\partial\Omega} = 5 + \frac{1}{2} \cdot 0 = 5$. Differentiation of u gives: $\frac{\partial u}{\partial n} = \frac{1}{2}\frac{\partial \omega}{\partial n}$. Since ω is a distance field normalized to the first order, its first normal derivative is 1 on the airfoil contour: $\frac{\partial \omega}{\partial n}\Big|_{\partial\Omega} = 1$. Therefore the first normal derivative of u takes on the prescribed value of $\frac{1}{2}$ on the airfoil contour.

Now consider a more general case when the values and derivatives prescribed over a geometric feature are functions of spatial variables. For example, suppose we would like to construct a function that satisfies the following conditions:

$$u|_{\partial\Omega} = 10x^2; \qquad \left.\frac{\partial u}{\partial n}\right|_{\partial\Omega} = 10 - 50(1 - 10y)\sin(100x). \tag{15}$$

The functions prescribed as boundary conditions (15) have to be "conditioned" before substitution into generalized Taylor series (6), so that they behave *as if* they were constant in the direction normal to the boundary (see equations (7) and (8) and discussion in Section 1.2). Conditioning is performed by the coordinate transformation $\mathbf{x} - \omega(\mathbf{x})\nabla\omega(\mathbf{x})$ that projects any point in space onto the geometric feature defined by distance field ω. This operation results in functions satisfying condition (7):

$$u_0^* = 10\left(x - \omega\frac{\partial \omega}{\partial x}\right)^2; \qquad u_1^* = 10 - 50\left(1 - 10\left(y - \omega\frac{\partial \omega}{\partial y}\right)\right)\sin\left(100\left(x - \omega\frac{\partial \omega}{\partial x}\right)\right). \tag{16}$$

Substituting these functions as coefficients into the generalized Taylor series (6) gives a function plotted in Figure 5(a). Similarly, we construct functions with specified second and higher order normal derivatives, but in this case the distance field that represents the geometry has to be normalized to the order of the highest derivatives. For example, the function shown in Figure 5(b), in addition to the conditions (15), satisfies the following condition on the second order normal derivative:

$$\left.\frac{\partial^2 u}{\partial n^2}\right|_{\partial\Omega} = 10^4 x. \tag{17}$$

To construct this function we used a distance field that is normalized to the second order (Figure 2(b)).

2.3 Material properties prescribed over multiple features

Usually, different material properties are prescribed over different geometric features in the same domain [2]. In this case, the global material composition is determined by interpolating contributions of individual material features using an inverse weighting distance technique. This classical method used for interpolation of scattered data, stands out because it interpolates the data using global functions without using any mesh or adjacency information among the given points. Shepard used the method in [26] for interpolation of meteorological and geographical/geological data in 1968, but Watson [33] cites much earlier applications of the same technique dating as far back as the 1920's;

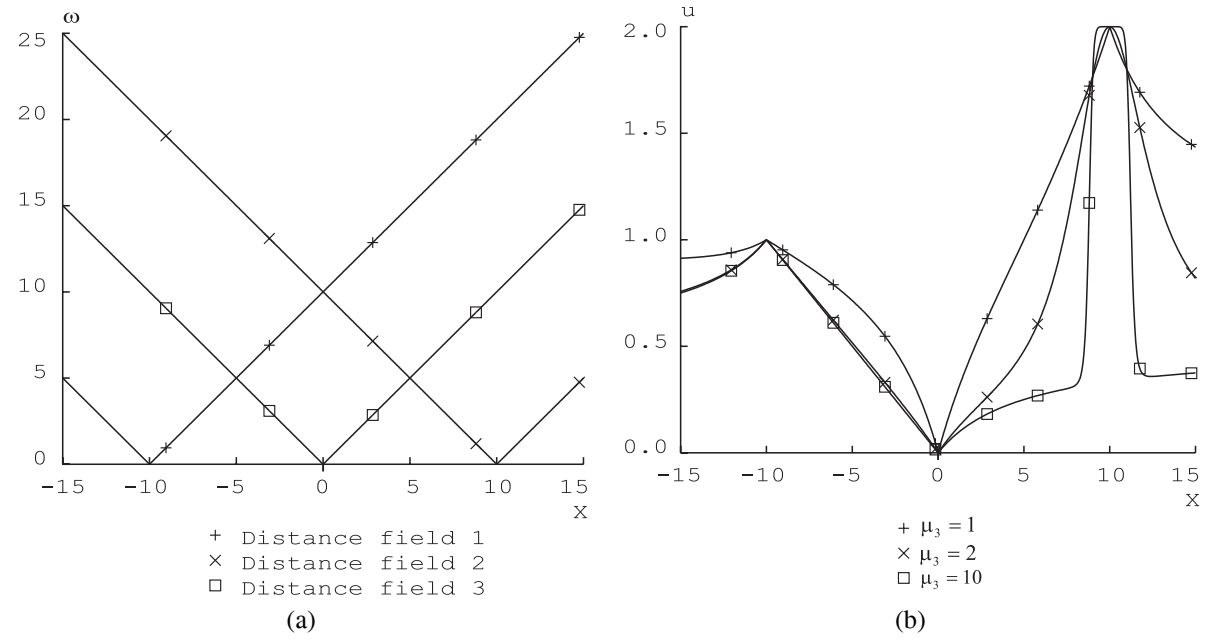

(a) (b)

Figure 6: (a) Distance fields used for interpolation of values prescribed at points $x_1 = -10$, $x_2 = 0$ and $x_3 = 10$. (b) Plots of the functions interpolating the values $u_1 = 1$, $u_2 = 0$ and $u_3 = 2$ prescribed at points $x_1 = -10$, $x_2 = 0$ and $x_3 = 10$ for $\mu_3 = 1, 2, 10$

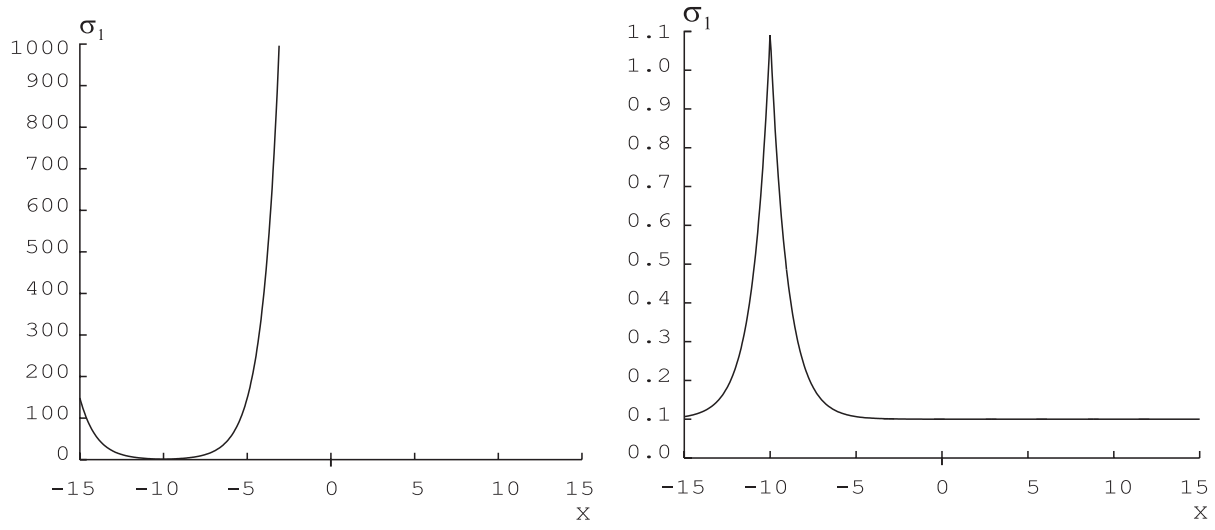

(a) (b)

Figure 7: Plot of the control functions σ_1: (a) $\sigma_1 = e^{\omega 1}$; (b) $\sigma_1 = 0.1 + e^{-\omega 1}$

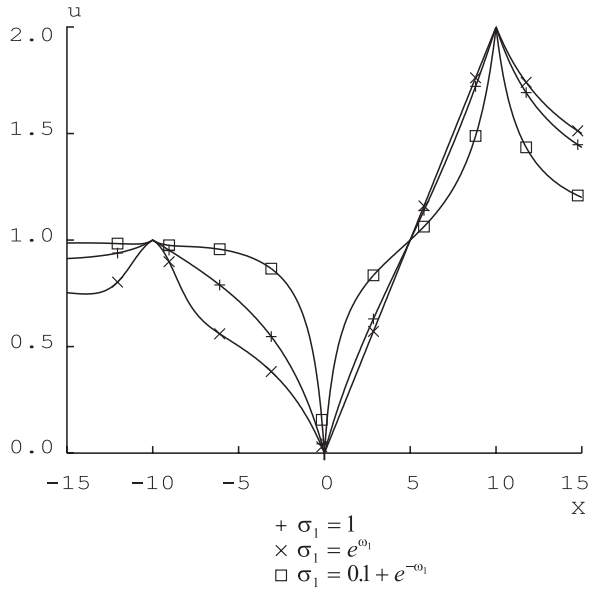

Figure 8: Plots of the functions interpolating the values $u_1 = 1$, $u_2 = 0$ and $u_3 = 2$ prescribed at points $x_1 = -10$, $x_2 = 0$ and $x_3 = 10$ for $\sigma_1 = 1$; $\sigma_1 = e^{\omega 1}$; and $\sigma_1 = 0.1 + e^{-\omega 1}$

Rvachev proposed a similar method for interpolating functions in 1967 [18]. In all cases, the interpolating function is constructed as a linear combination of the function's values u_i at points $\mathbf{x}$ with weight functions W_i:

$$u = \sum_{i=1}^{N} u_i W_i. \tag{18}$$

Each weight function W_i is inversely proportional to the distance from point $\mathbf{x}_i$ where the value u_i is prescribed. This expression can be considered as a representation of the function u in a basis formed by the functions $W_i(\mathbf{x})$. Therefore, we also expect that the weight functions W_i, $i = 1, ..., n$, should be positive continuous functions satisfying the interpolation condition $W_i(\mathbf{x}_j) = \delta_{ij}$ and forming a partition of unity, i.e. $\sum W_i(\mathbf{x}) = 1$. Many additional properties and variations of inverse distance weighting are discussed extensively in the literature [9, 33, 22]. In [2] we proposed to represent weights W_i in the following form:

$$W_i = \frac{\prod\limits_{j=1;j\neq i}^{N} (\sigma_j \omega_j)^{\mu_j}}{\sum\limits_{k=1}^{N} \prod\limits_{l=1;l\neq k}^{N} (\sigma_l \omega_l)^{\mu_l}} \tag{19}$$

This representation provides two sets of additional control parameters: $\{\mu_i\}_{i=1}^N$ and $\{\sigma_i\}_{i=1}^N$, that can be explained in terms of the classical problem of interpolating over the scattered points (nodes). It is well known [9] that the exponents μ_i control behavior of the interpolating function at the nodes: when $0 < \mu_i \leq 1$ the interpolant is not differentiable at the i-th node; values of $\mu_i > 1$ assure that the interpolant is differentiable $\mu_i - 1$ times at the i-th node, but it has a flat spot there. This fact is clearly illustrated by the plots presented in Figure 6(b). These functions interpolate values $u_1 = 1$, $u_2 = 0$ and $u_3 = 2$ prescribed at points $x_1 = -10$, $x_2 = 0$ and $x_3 = 10$. The weights $\{W_i\}_{i=1}^3$ are constructed using the distance fields shown in Figure 6(a) with $\sigma_1 = \sigma_2 = \sigma_3 = 1$ and $\mu_1 = \mu_2 = 1$. The functions whose plots are shown in Figure 6(b) differ from each other by the value of the exponent μ_3 that corresponds to the point $x = 10$: $\mu_3 = 1, 2, 10$. Figure 6(b) clearly shows that growth of exponent μ_3 results in a bigger flat spot at the point $x = 10$. The use of the exponents μ_i also makes it possible to interpolate the derivatives prescribed over the geometric features [21]. In such cases the value of the exponent μ_i associated with the ith geometric feature has to be

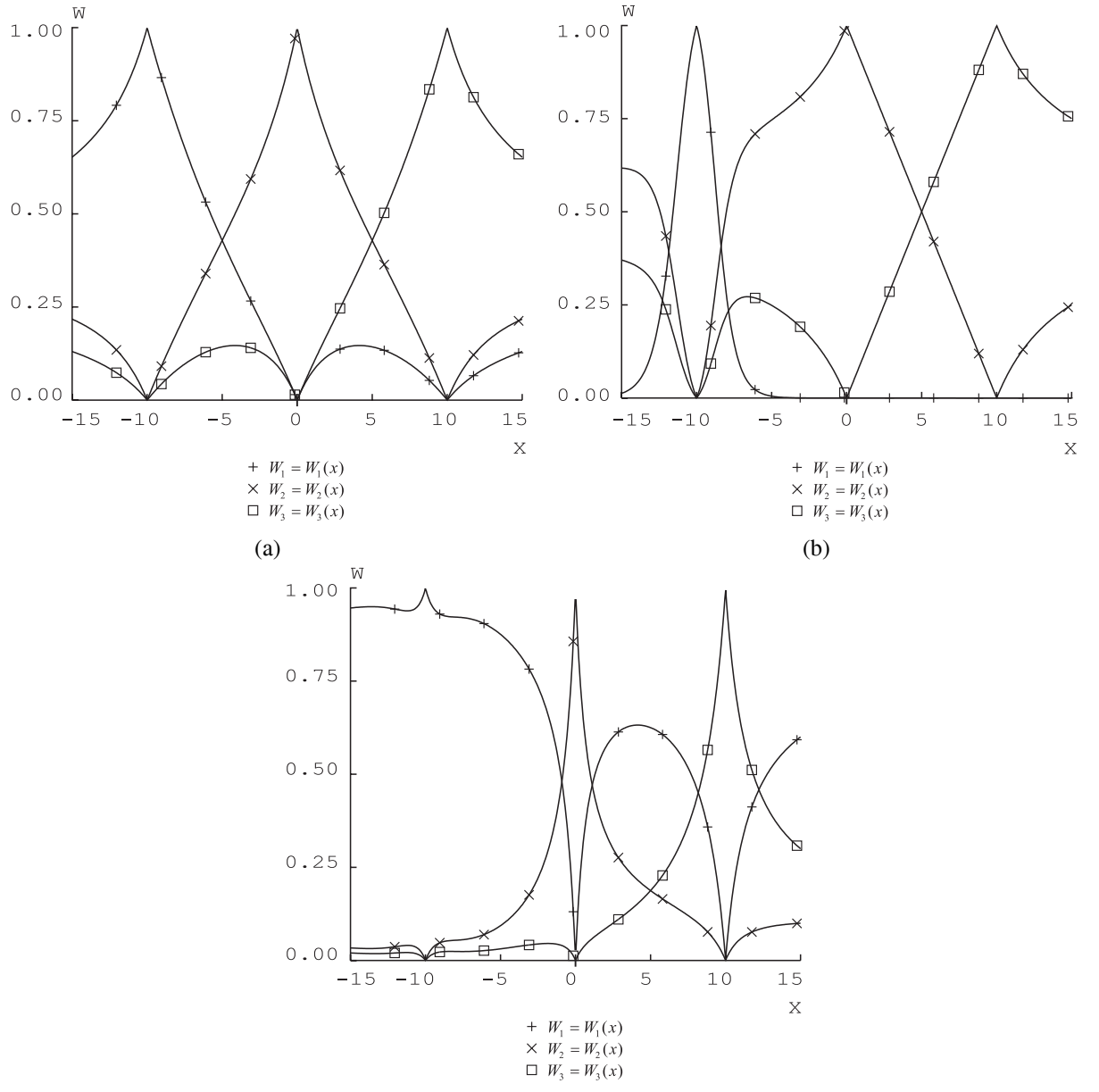

Figure 9: Interpolation weights $\{W_i\}_{i=1}^3$ (19) computed for the following sets of the control functions: (a) $\sigma_1 = \sigma_2 = \sigma_3 = 1$; (b) $\sigma_1 = e^{\omega 1}$, $\sigma_2 = \sigma_3 = 1$; (c) $\sigma_1 = 0.1 + e^{-\omega 1}$, $\sigma_2 = \sigma_3 = 1$.

one greater than the maximum order of the derivatives prescribed over that feature. Weights in the form (19) define the influence of the prescribed functions that decays at a rate inversely proportional to the product of functions σ_i and corresponding distance fields ω_i. Being strictly positive, functions σ_i control the decay of the weights W_i away of the geometric features. For example, if σ_1 is an increasing function of a distance as shown in Figure 7(a), weight W_1 exhibits fast decay away of the feature (Figure 9(b)). And vice versa, if σ_1 decays when the distance field increases, the decay of the weight W_1 is slower (Figure 9(c)). This fact allows us to use functions σ_i to control the influence zones of the functions prescribed over geometric features. The plots shown in Figure 8 illustrate that the influence zone in the neighborhood of the point $x = -10$ is narrower when σ_1 grows rapidly away of the point. In contrast, decaying function σ_1 whose plot is presented in Figure 7(b) results in a wider zone of influence.

In [21] we showed that this inverse distance weighting interpolation technique can be used to interpolate functions given over n-dimensional geometric features, and in [2] we used it to represent the variable properties of heterogeneous materials in 2D and 3D. For example, functions whose plots are shown in Figures 12(a), 12(b) and 12(c) represent the distribution of a thermal conductivity in a heterogeneous material in the cross section of the turbine blade shown in Figure 10. The turbine blade consists of a titanium insert coated by a heterogeneous material whose thermal conductivity varies from 7 $\frac{W}{m \cdot K}$ on the titanium insert to 150 $\frac{W}{m \cdot K}$ on the outer surface of the blade. The weights for interpolation are constructed using distance field ω_1 to the outer surface of the blade (Figure 11(a)) and distance field ω_2 to the titanium insert (Figure 11(b)). This means that ω_2 takes on zero value inside the region representing the insert and behaves as a distance to its boundary outside it. Since we prescribed no conditions on the derivatives of the thermal conductivity, we set the values of exponents μ_1 and μ_2 to 1. Function $\sigma_1 = e^{a\omega_1}$ controls the influence zone of the value prescribed on the outer surface of the blade. Plots presented in Figures 12(a), 12(b) and 12(c) correspond to $a = 1, 10^3, 10^4$. Higher values of coefficient a result in faster growth of σ_1 and consequently in faster decay of the conductivity away from the outer surface of the blade.

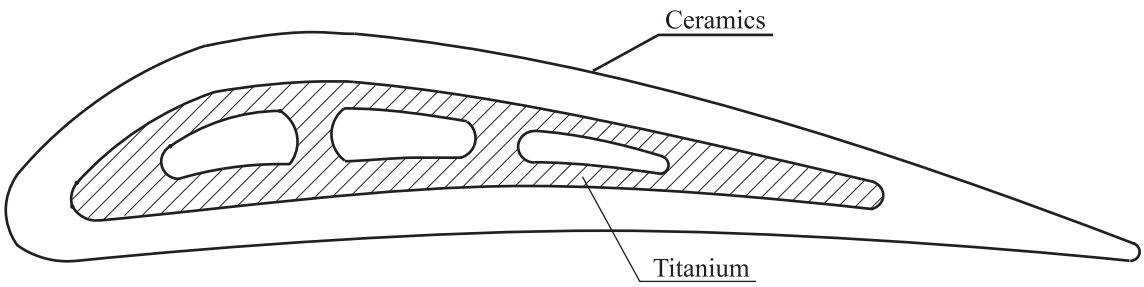

Figure 10: Cross section of a turbine blade: titanium insert surrounded by ceramics

2.4 Controlled material functions

Explicit control of material properties, as described above, may not be adequate for a number of reasons. Material distributions may not be specified in closed form because they usually must follow complex physical laws and constraints for which closed form solutions are not available. The generalized Taylor series, and the associated explicit power series, provide only an approximation of a material distribution with at least three distinct sources of errors. By definition, a generalized Taylor series expansion represents the function locally, in our case near the boundary of the material feature. Furthermore, explicit representation only approximates the material function when the remainder term is omitted. Finally, the accuracy of the generalized Taylor series depends on the accuracy of the distance field. Since we usually use only normalized (approximate) distance fields in order to assure differential properties, the accuracy of approximation may degrade substantially away from the feature.

Because the generalize Taylor series (6) applies to any and all functions, the remainder term may always be chosen to make the above inaccuracies arbitrarily small or to eliminate them altogether (recall Theorem 1). The errors are measured against one or more constraints on the material function specified either by the user or an application. Such constraints could be local or global, and may include algebraic, differential, or integral conditions that implicitly define the material function. For most such constraints, the remainder term cannot be determined exactly; therefore

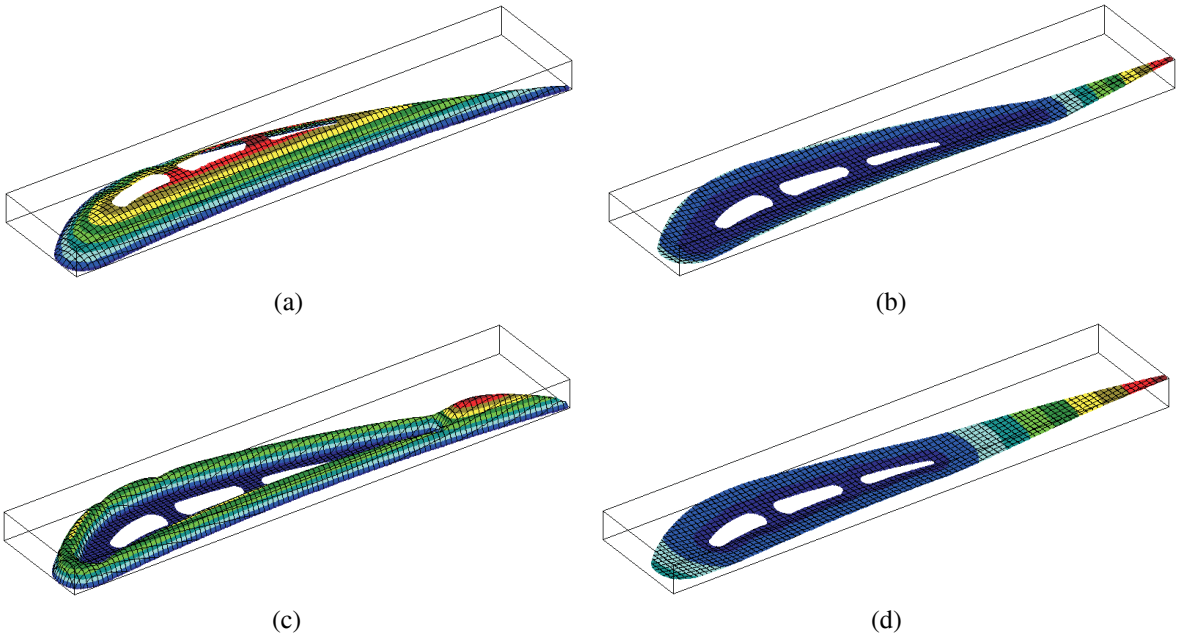

Figure 11: Approximate distance functions (a) to outer surface of the blade; (b) to the insert; (c) to outer surface of the blade and to the insert; (d) to the cooling channels

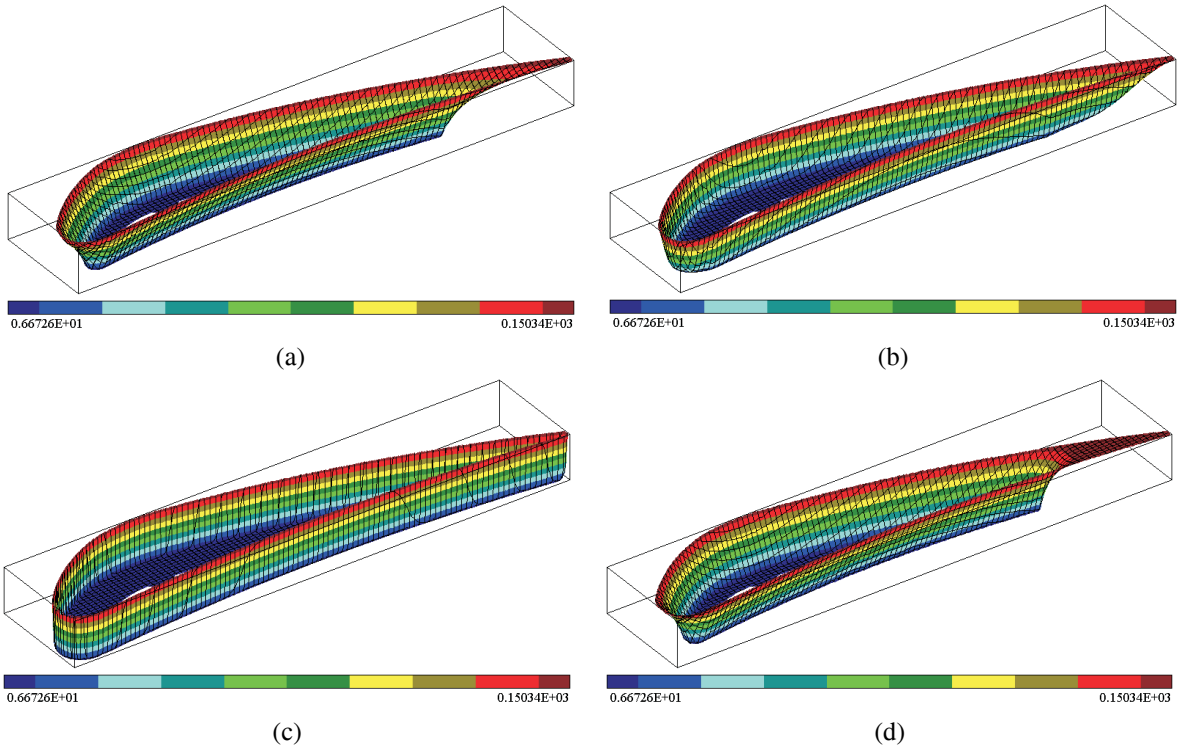

Figure 12: Functions interpolating the heat conduction with weights (a) $\sigma_1 = e^{\omega_1}$; $\sigma_2 = 1$; (b) $\sigma_1 = e^{10^3\omega_1}$; $\sigma_2 = 1$; (c) $\sigma_1 = e^{10^4\omega_1}$; $\sigma_2 = 1$. (d) Interpolating function that minimizes $\nabla\lambda$

we choose to represent the unknown function Φ in the remainder term $\omega^{m+1}\Phi$ by a linear combination

$$\Phi = \sum_{i=1}^{n} C_i \chi_i \tag{20}$$

of known basis functions χ_i from some sufficiently complete space, such as polynomials, B-splines, trigonometric polynomials, etc. Both errors and the basis functions χ_i are functions of spatial variables, and all modeling problems reduce to determination of the unknown coefficients C_i that enforce the prescribed constraints on the material function either exactly or approximately. Sometimes such constraints can be formulated as minimization of a functional. For example, thermal conductivity λ whose distribution is shown in Figure 12(d) minimizes the functional $F = \iint_{\Omega} (\nabla\lambda(p))^2 \, d\Omega$. The basis functions χ_i approximating the remainder are bicubic B-splines defined over a 60×60 uniform Cartesian grid. Figure 11(c) presents a plot of distance field ω in the remainder term.

3 Meshfree heat transfer in heterogeneous media

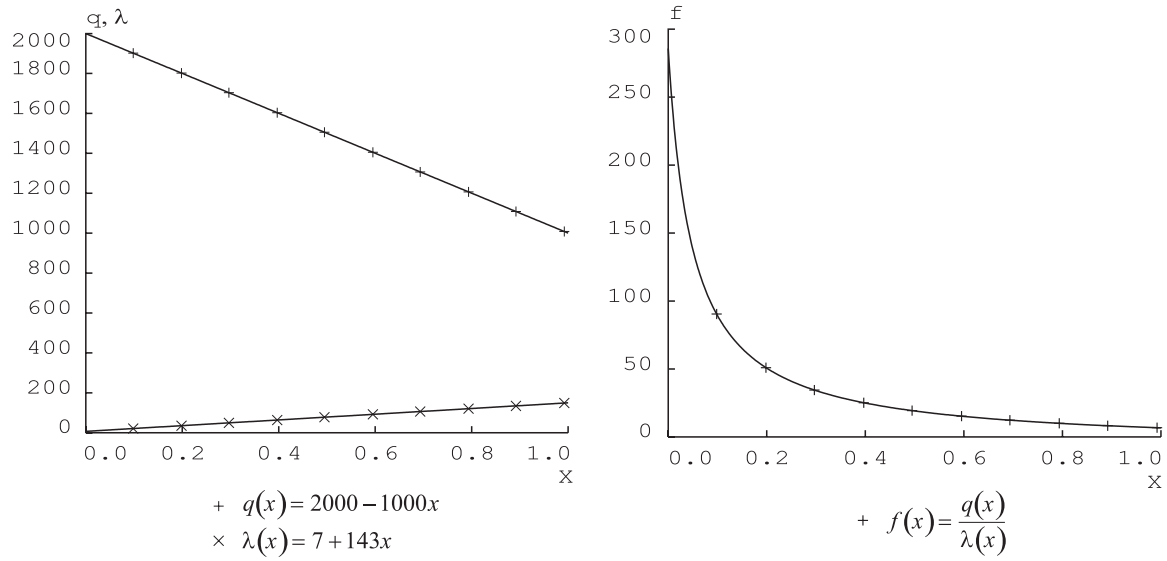

Figure 13: (a) Linear distributions of heat flux and thermal conductivity result in (b) a hyperbolic function as the boundary condition for the first normal derivative of temperature

3.1 RFM solution structures for variable material properties

One of the biggest challenges in modeling of physical fields on a computer is the treatment of prescribed boundary conditions because the solution of the problem must incorporate the analytic information about the boundary conditions as well as geometric information about boundaries where these conditions are specified. Variable material properties make this problem even more difficult because the variation of the material properties substantially affects the functions in the boundary conditions. For example, the Neumann boundary condition for a heat transfer problem is formulated as a ratio of the heat flux q and thermal conductivity λ:

$$\left.\frac{\partial u}{\partial n}\right|_{\partial\Omega} = \frac{q}{\lambda}. \tag{21}$$

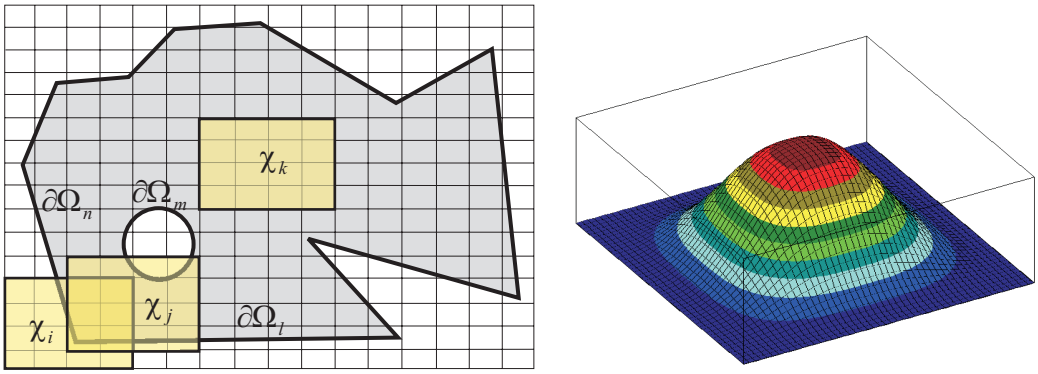

(a) (b)

Figure 14: (a) Compactly supported basis functions satisfy only those boundary conditions that are prescribed on the boundary pieces contained in the support. (b) B-spline basis function

Even if q and λ are linear functions of x: $q(x) = 2000 - 1000x$, $\lambda(x) = 7 + 143x$ (Figure 13(a)), their ratio defines a hyperbolic function whose plot is shown in Figure 13(b). This simple example suggests that satisfying boundary conditions requires taking into account the distribution of the physical properties of the heterogeneous medium as well as the other functions in the boundary conditions.

Rvachev proposed to employ the generalized Taylor series to construct solutions of boundary value problems that satisfy boundary conditions exactly. He introduced the term *solution structure* — an expression defining a space of functions that satisfy the prescribed boundary conditions. Solution structures for different boundary conditions can easily be derived from the generalized Taylor series. Let us show derivation of the solution structures satisfying the boundary conditions formulated for a second order partial differential equation. We already saw an example of solution structure (5) in Section 1 that satisfies Dirichlet boundary condition $u|_{\partial\Omega} = \varphi$ exactly. If different functions φ_i are prescribed on different boundaries $\partial\Omega_i$ they can be combined into one function φ via transfinite interpolation [21]. In this case the distance field ω in the solution structure (5) can be constructed from the individual distance fields ω_i using the methods described in [25, 32].

To derive the solution structure for Neumann boundary condition

$$\left.\frac{\partial u}{\partial n}\right|_{\partial\Omega} = \varphi, \tag{22}$$

where the function φ is a ratio of the heat flux and thermal conductivity λ (21); we expand u into a Taylor series by distance field ω:

$$u = u_0^* + u_1^*\omega + \omega^2\Phi_1. \tag{23}$$

As we discussed earlier, the coefficients u_0^* and u_1^* coincide with the prescribed value and first normal derivative of u on the boundary $\partial\Omega$. Since the Neumann boundary condition (22) does not restrict the value of u on the boundary $\partial\Omega$, we represent the first term in the Taylor series by the function Φ_2 that might be determined using additional constraints. The function Φ_2 must be conditioned to first order on the boundary $\partial\Omega$: $u_0^* = \Phi_2^* = \Phi_2 - \omega D_1^\omega(\Phi_2)$, where $D_1^\omega() = \nabla\omega \cdot \nabla()$ is the first order differential operator in the direction normal to the boundary. Recall that conditioning assures the constant behavior of u_0^* up to the normalization order of the distance field ω in the normal direction to the boundary $\partial\Omega$.

The function u_1^* represents the prescribed first normal derivative: $u_1^* = \left.\frac{\partial u}{\partial n}\right|_{\partial\Omega} = \varphi|_{\partial\Omega}$. Since the second and higher order derivatives of the function u are not specified on the boundary $\partial\Omega$, conditioning of the function φ is not required. Therefore, the solution structure satisfying the Neumann boundary condition appears as follows:

$$u = \Phi_2 - \omega D_1^\omega(\Phi_2) + \varphi\omega + \omega^2\Phi_1. \tag{24}$$

This solution structure contains two undetermined functions Φ_1 and Φ_2 each serving different purposes: the function Φ_2 approximates the value of u on the boundary of the domain, while Φ_1 assures the completeness of the solution structure.

The same approach can be used to derive a solution structure for a boundary condition of the third kind:

$$\left(\frac{\partial u}{\partial n} + hu\right)\Big|_{\partial\Omega} = \psi. \tag{25}$$

In the context of heat transfer problems, functions h and ψ in the boundary condition (25) incorporate the temperature of the environment $T_{env}(p)$, thermal conductivity $\lambda(p)$, and convective coefficient $\alpha(p)$: $h = \alpha(p)/\lambda(p)$ and $\psi(p) = \alpha(p)T_{env}(P)/\lambda(p)$, which are functions of spatial coordinates. First, we rewrite this boundary condition in the following form:

$$\frac{\partial u}{\partial n}\Big|_{\partial\Omega} = \psi - (hu)|_{\partial\Omega}\,, \tag{26}$$

and then repeat the derivation of the solution structure as described above. As a result, we obtain:

$$u = \Phi_2 - \omega D_1^{\omega}(\Phi_2) + \psi\omega - h\omega\Phi_2 + \omega^2\Phi_1. \tag{27}$$

Again, the undetermined function Φ_2 approximates the value of u on the boundary of the domain, and Φ_1 assures the completeness of the solution structure.

The solution structure for mixed boundary conditions

$$u|_{\partial\Omega_1} = \varphi; \qquad \left(\frac{\partial u}{\partial n} + hu\right)\Big|_{\partial\Omega_2} = \psi \tag{28}$$

is obtained via transfinite interpolation of the individual solution structures. Let u_1 and u_2 be functions satisfying Dirichlet and boundary conditions of the third kind respectively. Let us also assume that functions ω_1 and ω_2 are the distance fields to the boundaries $\partial\Omega_1$ and $\partial\Omega_2$. Then, application of transfinite interpolation (18) gives a function u that satisfies the mixed boundary conditions (28):

$$u = \frac{u_1\omega_2^2 + u_2\omega_1}{\omega_1 + \omega_2^2}. \tag{29}$$

Replacing functions u_1 and u_2 by their corresponding solution structures (5) and (27) results in:

$$u = \frac{1}{\omega_1 + \omega_2^2}\left(\left(\omega_1\Phi_1' + \varphi\right)\omega_2^2 + \left(\Phi_2 - \omega_2 D_1^{\omega_2}(\Phi_2) + \psi\omega_2 - h\omega_2\Phi_2 + \omega_2^2\Phi_3\right)\omega_1\right). \tag{30}$$

Let us combine the undetermined functions as $\Phi_1 = \Phi_1' + \Phi_3$. After substitution of Φ_1 into (30) and further simplification we obtain:

$$u = \frac{1}{\omega_1 + \omega_2^2}\left(\left(\omega_1\Phi_1 + \varphi\right)\omega_2^2 + \left(\Phi_2 - \omega_2 D_1^{\omega_2}(\Phi_2) + \psi\omega_2 - h\omega_2\Phi_2\right)\omega_1\right). \tag{31}$$

As we see, all solution structures include the following three components: (1) distance fields describing the boundaries where the boundary conditions are prescribed, (2) functions specified in the boundary conditions and (3) undetermined functions. The purpose of the undetermined functions is to satisfy additional constraints, for example, to approximate differential equation of a boundary value problem. Since in most situations the undetermined functions in the solution structures cannot be determined exactly, they are represented by linear combinations of basis functions (10).

Any solution structure can be split into homogeneous and non-homogeneous parts:

$$u = u_0 + u_1.$$

The non-homogeneous part u_1 satisfies the non-homogeneous boundary conditions, and contains the functions prescribed in the boundary conditions. The homogeneous part u_0 of the solution structure satisfies homogeneous boundary conditions, and contains all undetermined functions. For example, the solution structure for boundary conditions of the third kind (27) can be split into homogeneous and non-homogeneous parts as follows:

$$\begin{aligned} u_0 &= \Phi_2 - \omega D_1^{\omega}(\Phi_2) - h\omega\Phi_2 + \omega^2\Phi_1; \\ u_1 &= \psi\omega. \end{aligned} \tag{32}$$

Representing the unknown functions Φ_1 and Φ_2 by linear combinations of the basis functions:

$$\Phi_k = \sum_{i=1}^{N_k} C_{ki}\chi_{ki}, \quad k = 1, 2$$

we rewrite the homogeneous part u_0 of the solution structure (27) as follows:

$$u_0 = \sum_{i=1}^{N_2} C_{2i}\chi_{2i} - \omega D_1^{\omega}\left(\sum_{i=1}^{N_2} C_{2i}\chi_{2i}\right) - h\omega \sum_{i=1}^{N_2} C_{2i}\chi_{2i} + \omega^2 \sum_{j=1}^{N_1} C_{1j}\chi_{1j}. \tag{33}$$

After simplification we obtain:

$$u_0 = \sum_{i=1}^{N_2} C_{2i}\left(\chi_{2i} - \omega D_1^{\omega}\left(\chi_{2i}\right) - h\omega\chi_{2i}\right) + \sum_{j=1}^{N_1} C_{1j}\left(\omega^2\chi_{1j}\right). \tag{34}$$

Designating new basis functions as $\xi_{1i} = \omega^2\chi_{1i}$ and $\xi_{2i} = \chi_{2i} - \omega D_1^{\omega}\left(\chi_{2i}\right) - h\omega\chi_{2i}$ we represent the homogeneous part (34) of the solution structure (27) by a linear combination of the basis functions $\{\xi_{1i}\}_{i=1}^{N_1}$ and $\{\xi_{2i}\}_{i=1}^{N_2}$ satisfying homogeneous boundary condition:

$$u_0 = \sum_{i=1}^{N_1} C_{1i}\xi_{1i} + \sum_{j=1}^{N_2} C_{2j}\xi_{2j}. \tag{35}$$

Construction of the homogeneous part of the solution structure may also be considered a method for constructing basis functions that satisfy boundary conditions exactly. The solution structure can also be regarded as an operator that transforms *any* basis function χ into a basis function ξ that treats homogeneous boundary conditions exactly. Further, any complete system of the basis functions $\{\chi_i\}_{i=1}^{N}$ can be used: polynomials (classical, Chebyshev, Legendre, Bernstein, etc.), radial basis functions [11, 12, 5], B-splines [4], web-splines [7] and even finite elements. From a computational and an approximation point of view, it is advantageous to use basis functions defined over a finite support, for example, B-splines (Figure 14(b)).

Finite support allows us to localize computations, and therefore, substantially reduce the computational cost. Only those basis functions whose supports contain a given point are evaluated at that point. Furthermore, finite support allows us to localize construction of the solution structure, by taking into account only those boundary conditions that are prescribed on portions of the boundary that intersect the support of the particular basis function. Figure 14(a) explains this idea. To transform a basis function χ_i into a function ξ_i (these functions share the same support) satisfying the homogeneous boundary condition we need to use the information from only two boundaries $\partial\Omega_l$ and $\partial\Omega_n$. Similarly, function ξ_j, constructed from χ_j, satisfies the homogeneous boundary conditions given on boundaries $\partial\Omega_l$, $\partial\Omega_n$ and $\partial\Omega_m$. In other words, different solution structures are applied to the basis functions depending on the type of the boundary conditions prescribed on the boundaries which are completely or partially enclosed in the support of the particular basis function. The basis functions whose supports do not intersect the boundary of the geometric domain remain unchanged, i.e. $\xi_k = \chi_k$ (Figure 14(a)). Note that localization does not apply to the non-homogeneous part of the solution structure because the non-homogeneous part is a global function that interpolates non-homogeneous boundary conditions that are prescribed over all boundaries.

Solution structures for other types of boundary conditions can also be obtained using the generalized Taylor series. The above examples were derived manually largely for the benefit of the reader. In [32] we showed that construction of the solution structures can be automated completely, and it could be performed at run time.

3.2 Solution method

The concept of a solution structure provides a mathematical means for exact treatment of boundary conditions. However, in most cases the differential equation of the problem cannot be satisfied exactly. Therefore, the solution procedure must determine numerical values for the coefficients in the solution structure so that it approximates the differential equation. RFM does not place any restrictions on the solution method, and therefore, can be used to enhance any other solution method for boundary value problems, by providing exact treatment of boundary conditions. Until now, RFM has been mostly developed in conjunction with variational methods because it provides a very natural extension to them. Below we explain several such solution procedures in the context of modeling temperature fields in heterogeneous media with continuously varying physical properties.

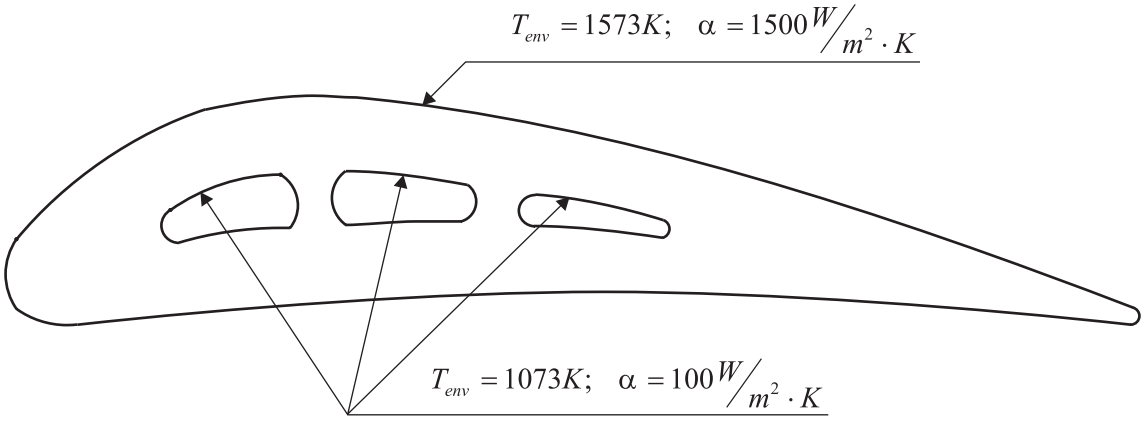

Figure 15: Boundary conditions on the outer surface of the turbine blade and on the surface of the cooling channels

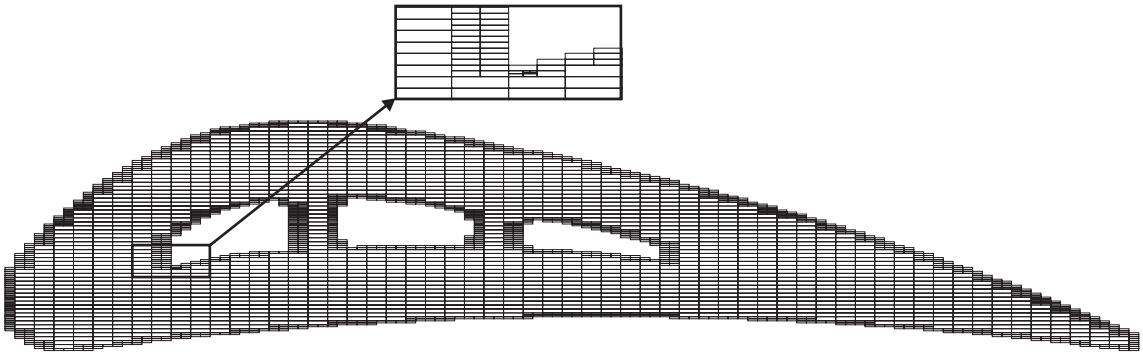

(a)

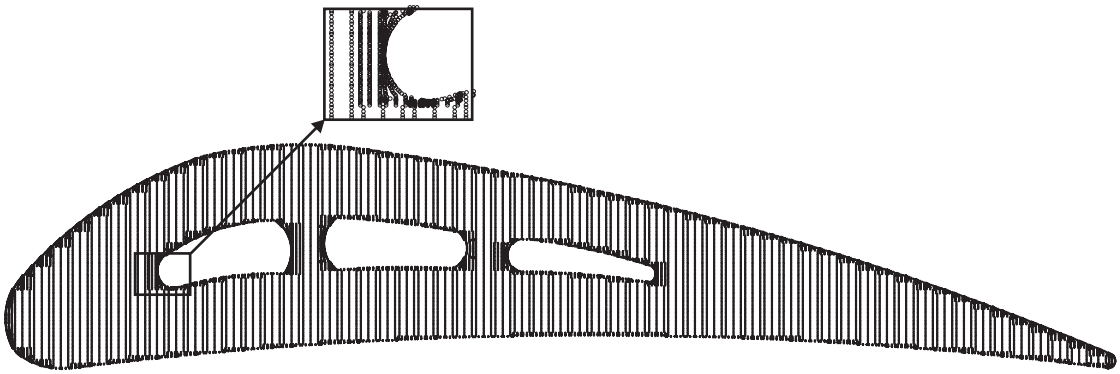

(b)

Figure 16: Adaptive integration employs hierarchical space decomposition of the geometric model

Numerical formulation Since the heat transfer problem is positive definite, we can employ the classical Ritz method. Application of this method to differential equation (3) with mixed boundary conditions

$$u|_{\partial\Omega_1} = T_1; \qquad \left(\frac{\partial u}{\partial n} + \frac{\alpha}{\lambda(p)}u\right)\Big|_{\partial\Omega_2} = \frac{\alpha T_2}{\lambda(p)} \tag{36}$$

leads to a system of linear algebraic equations $\mathbf{AC} = \mathbf{B}$. Elements of the matrix $\mathbf{A}$ and the vector $\mathbf{B}$ are given by the following expressions:

$$\begin{aligned} a_{ij} &= \iint\limits_{\Omega} \lambda(p)\left(\nabla\xi_i \cdot \nabla\xi_j\right) d\Omega + \int\limits_{\partial\Omega} \frac{\alpha}{\lambda(p)}\xi_i\xi_j dS; \\ b_i &= -\iint\limits_{\Omega} \lambda(p)\left(\nabla\xi_i \cdot \nabla u_1\right) d\Omega + \int\limits_{\partial\Omega} \frac{\alpha}{\lambda(p)}\left(T_2 - u_1\right)\xi_i dS; \end{aligned} \tag{37}$$

where $\{\xi_i\}_{i=1}^N$ are basis functions satisfying the homogeneous boundary conditions; u_1 is a function that satisfies the non-homogeneous boundary conditions; α is a convection coefficient; and $\lambda(p)$ is a thermal conductivity of a heterogeneous media. Employing Green's formula, the Ritz functional applied to a partial differential equation with variable coefficients (3) naturally treats the term $\nabla\lambda(p)\nabla u$. Therefore the expressions (37) contain the same terms as in the case of homogeneous medium. The only difference is that the thermal conductivity $\lambda(p)$ is a function of spatial coordinates. Application of other methods, for example a least square method, may result in the matrices and vectors whose elements depend on the gradient of the thermal conductivity $\lambda(p)$:

$$\begin{aligned} a_{ij} &= \iint\limits_{\Omega} \left(\lambda(p)\nabla^2\xi_i + \nabla\lambda(p)\nabla\xi_i\right)\left(\lambda(p)\nabla^2\xi_j + \nabla\lambda(p)\nabla\xi_j\right) dS; \\ b_i &= -\iint\limits_{\Omega} \left(\lambda(p)\nabla^2\xi_i + \nabla\lambda(p)\nabla\xi_i\right)\left(\lambda(p)\nabla^2 u_1 + \nabla\lambda(p)\nabla u_1\right) dS. \end{aligned} \tag{38}$$

Adaptive Integration Expressions (37) and (38) show that elements of the matrix and vector are obtained by integration of expressions containing products of the basis functions, their partial derivatives, functions prescribed as boundary conditions, and functions describing the physical properties of the medium. Since neither the functions nor the geometric shapes are known a priori, analytic computations are difficult and impractical. To compute the partial derivatives in expressions (37) and (38) we employ the automatic differentiation technique described in [30, 31]. Mesh-based integration techniques discretize the geometric domain *a priori* in order to perform numerical integration. In contrast, meshfree methods construct the data structure for the integration as well as the functions to be integrated at run time. The absence of the spatial grid on one hand makes integration difficult, but on the other hand meshfree methods can employ flexible adaptive integration algorithms that use the original geometry to allocate the integration points.

Adaptivity to the geometrical shape of the domain is achieved by proper placement of the integration points. Geometrically adaptive algorithms described in [32] rely on hierarchical space partitioning similar to quad/octree decompositions. Figure 16(a) illustrates hierarchical space partition for the geometric domain in Figure 15. Initially, the whole space is covered by a uniform Cartesian grid (60×60) that coincides with the B-splines grid. Then the cells that are completely located outside the domain are removed, and the cells that intersect the boundary of the domain are hierarchically subdivided (Figure 16(a)). Once the cells are subdivided the integration points are allocated inside the cells according to the integration rules as shown in Figure 16(b). The original geometric model is used to ensure that no integration point is placed outside the geometric domain.

Adaptivity to the integrand is achieved by varying the number of integration points inside a cell. It requires error estimation in conjunction with a divide-and-conquer approach. Error estimators are known for most integration rules. Newton-Cotes integration rules estimate the integration error by computing the integral twice: first, using the given number of the integration points, and then using half of them. Simple formulas translate the difference between computed integrals into the integration error. The Gauss-Kronrod extension [14] of the Gaussian integration rules provides the error estimation for the integration rules that are mostly used by engineering analysis methods. If the integration error provided by the error estimator is greater than prescribed, additional integration points are allocated.

For some functions this strategy could result in infinitely many integration points, and any practical implementation must limit the maximum number of the integration points in a cell. If this limit is exceeded, the cell is subdivided and integration points are allocated in each subcell.

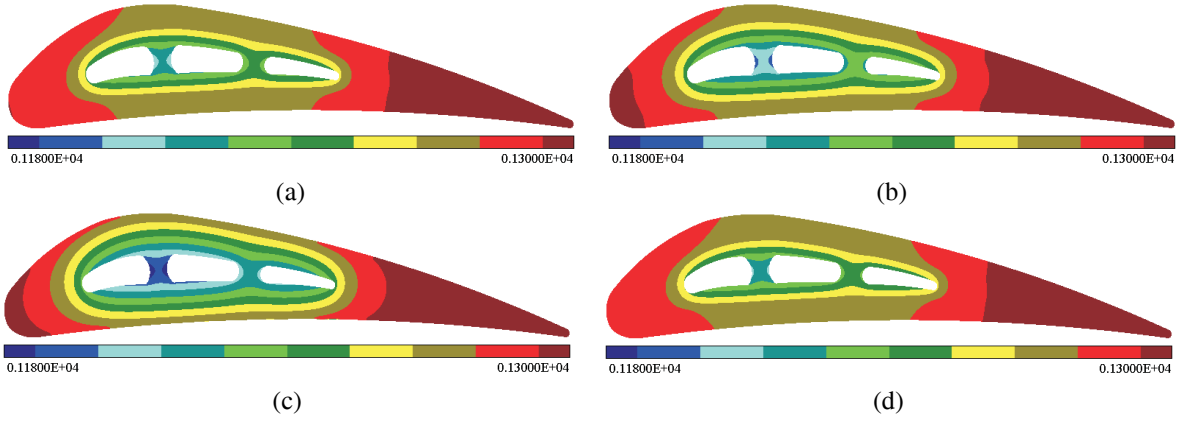

Figure 17: Temperature distributions computed for variations of the thermal conductivity presented in Figure 12

Example Let us model the distribution of a temperature field in the cross section of a turbine blade that is shown in Figure 10. The solution steps shown are fully automated by the described meshfree method and require no manual intervention from the user. The heat exchange with the environment is described by convective boundary conditions:

$$\left(\frac{\partial u}{\partial n} + \frac{\alpha}{\lambda(p)}u\right)\Big|_{\partial\Omega} = \frac{\alpha T_{env}}{\lambda(p)}, \tag{39}$$

where the convective coefficient α and the temperature of the environment T_{env} are prescribed on the cooling channels and the outer surface of the blade as shown in Figure 15:

$$\alpha|_{\partial\Omega_1} = 100\frac{W}{m^2 \cdot K}; \qquad \alpha|_{\partial\Omega_2} = 1500\frac{W}{m^2 \cdot K}; \tag{40}$$

$$T_{env}|_{\partial\Omega_1} = 1073K; \qquad T_{env}|_{\partial\Omega_2} = 1573K. \tag{41}$$

Using transfinite interpolation we construct functions α and T_{env} that satisfy conditions (40) and (41) respectively:

$$\begin{aligned} \alpha &= \frac{100\omega_2 + 1500\omega_1}{\omega_1 + \omega_2}; \\ T_{env} &= \frac{1073\omega_2 + 1573\omega_1}{\omega_1 + \omega_2}, \end{aligned} \tag{42}$$

where ω_1 and ω_2 are distance fields to the cooling channels and the outer surface of the blade. Plots of the functions ω_1 and ω_2 are shown in Figure 11(d) and Figure 11(a) respectively. The solution structure (27) represents a function satisfying the boundary condition (39). Substituting expressions (42) into boundary conditions (39), we obtain expressions for functions h and ψ in the solution structure (27):

$$h = \frac{100\omega_2 + 1500\omega_1}{\lambda(p)(\omega_1 + \omega_2)};$$

$$\psi = \frac{(100\omega_2 + 1500\omega_1)(1073\omega_2 + 1573\omega_1)}{\lambda(p)(\omega_1 + \omega_2)^2}.$$

We will model the distributions of the temperature field using the previously computed distributions of thermal conductivity $\lambda(p)$ as shown in Figure 12.

Application of the Ritz method to the differential equation (3) with the given boundary conditions (39) results in an algebraic system $\mathbf{AC} = \mathbf{B}$ whose elements are computed as follows:

$$
\begin{aligned}
a_{ij} &= \iint\limits_{\Omega} \lambda(p)\left(\nabla\xi_i \cdot \nabla\xi_j\right) d\Omega + \int\limits_{\partial\Omega} \frac{100\omega_2 + 1500\omega_1}{\lambda(p)(\omega_1+\omega_2)}\xi_i\xi_j dS; \\
b_i &= -\iint\limits_{\Omega} \lambda(p)\left(\nabla\xi_i \cdot \nabla\left(\omega\frac{(100\omega_2 + 1500\omega_1)(1073\omega_2 + 1573\omega_1)}{\lambda(p)(\omega_1+\omega_2)^2}\right)\right) d\Omega + \\
&\int\limits_{\partial\Omega} \frac{(100\omega_2 + 1500\omega_1)(1073\omega_2 + 1573\omega_1)}{\lambda(p)(\omega_1+\omega_2)^2}\xi_i dS,
\end{aligned}
\tag{43}
$$

where the function ω is a distance field to the cooling channels and the outer surface of the blade. Having solved the system of linear algebraic equations, we substitute the numerical values of the coefficients C_i into the solution structure (27). We will evaluate the solution structure at various points to visualize the temperature field. Figure 17 shows the temperature fields for the thermal conductivities shown in Figure 12.

3.3 Temperature field in piecewise heterogeneous materials

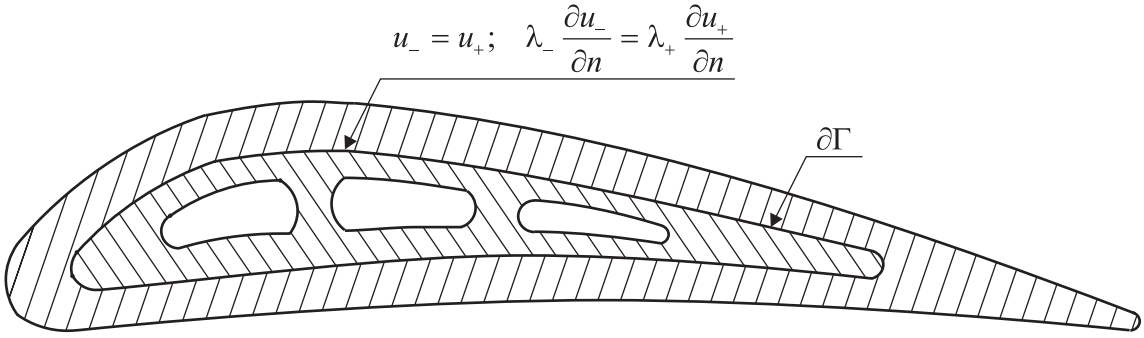

Figure 18: Boundary conditions of an ideal thermal contact are prescribed on the material interface

A special case of the material heterogeneity is a contact of media with different physical properties. This causes discontinuities of the physical properties across the boundary of the contact, generally referred to as the *interface.* The corresponding mathematical model requires additional interface boundary conditions. The mathematical formulation of such boundary conditions depends on the type of the physical problem. In the case of heat transfer, the heat exchange on the contact boundary is described by a boundary condition of an ideal thermal contact requiring equality of temperatures and heat fluxes on opposite sides of the interface boundary (Figure 18):

$$
\begin{aligned}
u_-\big|_{\partial\Gamma} &= u_+\big|_{\partial\Gamma}; \\
\lambda_- \frac{\partial u_-}{\partial n}\bigg|_{\partial\Gamma} &= \lambda_+ \frac{\partial u_+}{\partial n}\bigg|_{\partial\Gamma}.
\end{aligned}
\tag{44}
$$

Here the subscripts "-" and "+" designate the values of the temperature u and thermal conductivity λ on opposite sides of the interface.

Generally speaking, interface boundary conditions complicate the solution procedures because they introduce discontinuities in the physical field and/or derivatives (gradient, curvature, etc.) Boundary condition of the ideal thermal contact (44) results in a discontinuity in the temperature gradient along the interface boundary, measured by the ratio of the thermal conductivities on opposite sides of the interface boundary. The greater the ratio of the thermal conductivities, the greater is the discontinuity in the temperature gradient. Such discontinuities must be built into the corresponding solution structure. We now show how this can be accomplished using normalized distance fields. Let

u be a solution structure that satisfies boundary conditions given on the boundary $\partial\Omega$ described by the distance field ω. Let γ be a distance field to the interface boundary. Then the solution structure that satisfies both the interface condition of ideal thermal contact (44) as well as the boundary condition prescribed on $\partial\Omega$ is represented by the following expression [29]:

$$u_{\pm} = u + \delta_{\pm}\omega' D_1^{\gamma}(u), \tag{45}$$

where the subscript "$\pm$" designates the solution structures u_{-} or u_{+} as well as their elements on the opposite sides of the interface boundary; ω' is a normalized function on the interface boundary $\partial\Gamma$ that has zero value and zero first normal derivative on the boundary $\partial\Omega$. In other words, expression (45) defines two solution structures acting on the opposite sides of the boundary $\partial\Gamma$. Because $\omega' = 0$ on the interface boundary $\partial\Gamma$, the continuity condition on the temperature $u_{-}\big|_{\partial\Gamma} = u_{+}\big|_{\partial\Gamma}$ is automatically satisfied. The condition $\frac{\partial\omega'}{\partial n}\Big|_{\partial\Omega} = 0$ assures that the terms $\delta_{\pm}\omega' D_1^{\gamma}(u)$ do not affect the boundary conditions prescribed at $\partial\Omega$. Values of the constants $\delta_{\pm}$ need to be chosen in such a way that the continuity of the heat flux is satisfied on the boundary $\partial\Gamma$. In order to determine numerical values of $\delta_{\pm}$ we substitute the solution structure (45) into the heat flux continuity condition. After simplification we obtain:

$$\lambda_{-}\left(1+\delta_{-}\right) = \lambda_{+}\left(1+\delta_{+}\right). \tag{46}$$

Then we transform (46) into the following expression:

$$\frac{\lambda_{-}}{\lambda_{+}} = \frac{1+\delta_{+}}{1+\delta_{-}} \tag{47}$$

from which we obtain the values of the constants $\delta_{\pm}$:

$$\delta_{\pm} = M\lambda_{\mp} - 1, \tag{48}$$

where M is an arbitrary constant. It follows from expression (47) there exist infinitely many pairs of coefficients $\delta_{\pm}$ satisfying condition (47). For definiteness let us restrict the values of $\delta_{\pm}$ by inequalities:

$$-1 < \delta_{-} \leq 1;$$

$$-1 < \delta_{+} \leq 1.$$

These additional conditions constrain the value of the constant M in the expression (48) [29]:

$$0 < M \leq \min\left\{\frac{2}{\lambda_{-}}, \frac{2}{\lambda_{+}}\right\}. \tag{49}$$

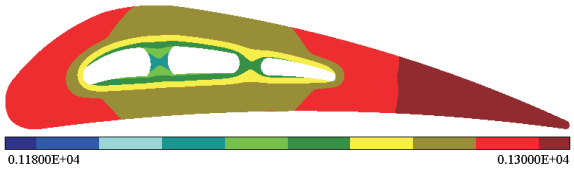

Figure 19: Temperature field in turbine blade

Example Let us model the distribution of the temperature field in the cross section of the turbine blade. The blade consist of the titanium insert coated with a ceramic material as shown in Figure 10. The thermal conductivities of the titanium and ceramic are 7 $\frac{W}{m\cdot K}$ and 150 $\frac{W}{m\cdot K}$ respectively. To model the temperature distribution we will use the boundary condition (39) from the example discussed in Section 3.2. Therefore we will use the same solution structure (27) that satisfies boundary condition (39) exactly. In order to satisfy the interface condition (44) of an ideal thermal contact, we apply the solution structure (45) to the function u given by expression (27). Now let us determine numerical values for the coefficients $\delta_{\pm}$ in the solution structure (45). Assume that the "-" subscript corresponds to

the titanium insert, and the "+" corresponds to the ceramic coating. With this convention, we have $\lambda_- = 7\,\frac{W}{m\cdot K}$ and $\lambda_+ = 150\,\frac{W}{m\cdot K}$. Then the constant M has the value of $M = \min\{\frac{2}{7}, \frac{2}{150}\} = \frac{2}{150}$. Substituting this value of M into (48) we obtain the following values for the coefficients $\delta_\pm$: $\delta_- = M\lambda_+ - 1 = \frac{2}{150}\cdot 150 - 1 = 1$ and $\delta_+ = M\lambda_- - 1 = \frac{2}{150}\cdot 7 - 1 = -\frac{136}{150}$. Application of the Ritz method results in the temperature field whose isolines are presented in Figure 19.

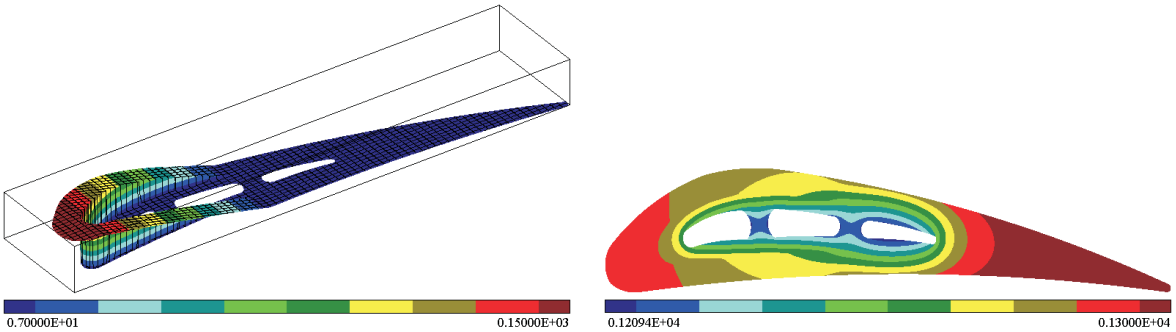

(a) (b)

Figure 20: (a) Distribution of the thermal conductivity with discontinuities along the interface boundary; and (b) temperature field computed for heterogeneous heat conductivity presented in Figure 20(a)

4 Conclusions and future directions

In this paper we showed application of the meshfree RFM to the modeling of temperature fields in heterogeneous media. We explained and demonstrated the method with examples of two cases of material heterogeneity: continuous and discrete. It should be clear that the two cases are not mutually exclusive, and the proposed approach may also be used in the general case where the material properties are variable throughout the volume with discontinuities along an interface boundary. For example, Figure 20(b) shows isolines of the temperature field computed for the distribution of the variable thermal conductivity whose plot is shown in Figure 20(a). The thermal conductivity shown in Figure 20(a) is continuous on a portion of the interface boundary $\partial\Gamma$ (Figure 18) and is discontinuous across the rest of the interface.

Intuitively, the described method parameterizes all functions by distances to the boundaries and interfaces of the geometric domain. The distance fields themselves can also be parameterized by the design parameters of a geometric model. As a result, all functions of the distance fields become parameterized by geometric design parameters. This simplifies sensitivity analysis because the physical fields that are explicit functions of the design parameters can be easily differentiated with respect to the design parameters using either symbolic [34] or automatic [30, 31] differentiation methods. Representation of the physical properties of heterogeneous media by functions of the distances makes their control easy and intuitive [2]. Further, representing the physical properties in the same form as other physical fields unifies field modeling problems, and makes it possible to apply the same solution methods and algorithms to optimization of the physical properties of heterogeneous media in the same computational environment. Designers can interactively change the control parameters of the material properties and see the response of physical fields to such changes. In this sense, physical properties of heterogeneous media become design parameters, which opens the possibility of carrying out integrated shape-material optimization.

From a computational point of view, the intrinsic advantage of the described meshfree method is in the clean and modular separation of the geometric information represented by function ω from the differential equation and the numerical method used to determine the unknown function Φ. This separation supports complete automation of the solution procedure as described in [32] and demonstrated by the Semi-Analytic Geometry Engine (SAGE) – the computer system providing meshfree heat transfer and plate natural vibration. SAGE has been developed at Spatial Automation Laboratory of University of Wisconsin-Madison, and it is available for public use from http://sal-cnc.me.wisc.edu. The solution procedure also requires computation of partial derivatives of functions and their integration over the geo-

metric model. In order to compute the partial derivatives of functions constructed at run time we developed automatic differentiation algorithms. These algorithms are implemented in the Fast Forward Automatic Differentiation Library (FFADLib) [30, 31], available for public use from http://sal-cnc.me.wisc.edu.

The 2D heat transfer examples in this paper were chosen for their simplicity, but the method generalizes fully to 3D domains and more complex problems. Currently, we are applying the meshfree method to other physical problems in heterogeneous media including linear elasticity and thermo-elasticity. Extension of the method into 3D requires construction of the distance fields for 3D geometric models, and development of adaptive 3D volume and surface integration algorithms. In this paper we constructed all distance fields for the boundaries of the geometric model using R-functions. We showed in [25, 32] that normalized distance fields with guaranteed differential properties can be constructed automatically from standard geometric representations. But the proposed meshfree method can be used with distance fields constructed by other methods and does not depend on R-functions per se. For example, in [6] we demonstrated automated meshfree 3D analysis with distance fields that are sampled from either engineered or captured data.

Acknowledgments

This research is supported in part by the National Science Foundation grants DMI-0115133, and CCR-0112758, DMI-0323514, and the National Institute of Standards (NIST) grant 60NANB2D0126.

References

[1] A. Biswas and V. Shapiro. Approximate distance fields with non-vanishing gradients. *Graphical Models*, 2004. to appear.

[2] A. Biswas, V. Shapiro, and I. Tsukanov. Heterogeneous material modeling with distance fields. *Computer Aided Geometric Design*, 21(3):215–242, 2004.

[3] W. Cho, E. M. Sachs, N. M. Patrikalakis, M. Cima, H. Liu, J. Serdy, and C. C. Stratton. Local composition control in solid freeform fabrication. In *Proceedings of the 2002 NSF Design, Service and Manufacturing Grantees and Research Conference*, San Juan, Puerto Rico, January 2002.

[4] Carl de Boor. *A Practical Guide to Splines*. Springer-Verlag, 2001.

[5] A.I. Fedoseyev, M. J. Friedman, and E.J. Kansa. Improved multiquadric method for elliptic partial differential equations via pde collocation on the boundary. *Computers and Mathematics with Applications*, 43(3-5):491–500, 2001.

[6] M. Freytag, V. Shapiro, and I. Tsukanov. Field modeling with sampled data. Technical report 2004-1, Spatial Automation Laboratory, http://sal-cnc.me.wisc.edu, 2004.

[7] K. Hollig. *Finite Element Methods with B-Splines*. Number 26 in Frontiers in Applied Mathematics. SIAM, 2003.

[8] J. B. Holt, M. Koizumi, T. Hirai, and Z. A. Munir, editors. *Ceramic Transactions*, volume 34. The American Ceramic Society, Westerville, Ohio, 1993.

[9] J. Hoschek and D. Lasser. *Fundamentals of Computer Aided Geometric Design*. A K Peters, 1993.

[10] T. R. Jackson. *Analysis of Functionally Graded Material Object Representation Methods*. PhD thesis, MIT, Ocean Engineering Department, June 2000.

[11] E. J. Kansa. Multiquadrics – a scattered data approximation scheme with applications to computational fluid dynamics: I. Surface approximations and partial derivative estimates. *Computers and Mathematics with Applications*, 19(6-8):127–145, 1990.

[12] E. J. Kansa. Multiquadrics – a scattered data approximation scheme with applications to computational fluid dynamics: II. Solutions to parabolic, hyperbolic, and elliptic partial differential equations. *Computers and Mathematics with Applications*, 19(6-8):147–161, 1990.

[13] L. V. Kantorovich and V. I. Krylov. *Approximate Methods of Higher Analysis*. Interscience Publishers, 1958.

[14] A. S. Kronrod. *Nodes and Weights of Quadrature Formulas: Sixteen place tables*. Consultants Bureau, New York, 1965.

[15] Hongye Liu, Wonjoon Cho, Todd R. Jackson, Nicholas M. Patrikalakis, and Emanuel M. Sachs. Algorithms for design and interrogation of functionally gradient material objects. In *Proceedings of ASME 2000 IDETC/CIE 2000 ASME Design Automation Conference*, Baltimore, MD, 2000.

[16] Yoshinari Miyamoto, W. A. Kaysser, and B. H. Rabin, editors. *Functionally Graded Materials: Design, Processing and Applications.* Kluwer Academic Publishers, Boston, 1999.

[17] X. Qian and D. Dutta. Design of heterogeneous turbine blade. *Computer-Aided Design*, 35:319–329, 2003.

[18] V. L. Rvachev. *Geometric Applications of Logic Algebra*. Naukova Dumka, 1967. In Russian.

[19] V. L. Rvachev. *Theory of R-functions and Some Applications*. Naukova Dumka, 1982. In Russian.

[20] V. L. Rvachev, T. I. Sheiko, V. Shapiro, and I. Tsukanov. On completeness of RFM solution structures. *Computational Mechanics*, 25:305–316, 2000.

[21] V. L. Rvachev, T. I. Sheiko, V. Shapiro, and I. Tsukanov. Transfinite interpolation over implicitly defined sets. *Computer Aided Geometric Design*, 18:195–220, 2001.

[22] N. S. Sapidis. *Designing fair curves and surfaces: shape quality in geometric modeling and computer-aided design*. SIAM, 1994.

[23] V. Shapiro. Theory of R-functions and applications: A primer. Technical Report CPA88-3, Cornell University, November 1988.

[24] V. Shapiro. Real functions for representation of rigid solids. *Computer-Aided Geometric Design*, 11(2):153–175, 1994.

[25] V. Shapiro and I. Tsukanov. Implicit functions with guaranteed differential properties. In *Fifth ACM Symposium on Solid Modeling and Applications*, Ann Arbor, MI, 1999.

[26] D. Shepard. A two-dimensional interpolation function for irregularly spaced data. In *Proceedings 23rd ACM National Conference*, pages 517–524, 1968.

[27] Y. K. Siu and S. T. Tan. Modeling the material grading and structures of heterogeneous objects for layered manufacturing. *Computer-Aided Design*, 34:705–716, September 2002.

[28] Y. K. Siu and S. T. Tan. Source-based heterogeneous solid modeling. *Computer-Aided Design*, 34:41–55, January 2002.

[29] Yu. G. Stoian, V. S. Protsenko, and G. P. Manko. *Theory of R-functions and Actual Problems of Applied Mathematics*. Naukova Dumka, 1986. In Russian.

[30] I. Tsukanov and M. Hall. Fast Forward Automatic Differentiation Library (FFADLib): A User Manual. Tech. report 2000-4, Spatial Automation Laboratory, http://sal-cnc.me.wisc.edu, 2000.

[31] I. Tsukanov and M. Hall. Data structure and algorithms for fast automatic differentiation. *International Journal for Numerical Methods in Engineering*, 56(13):1949–1972, April 2003.

[32] I. Tsukanov and V. Shapiro. The architecture of SAGE – a meshfree system based on RFM. *Engineering with Computers*, 18(4):295–311, 2002.

[33] D. F. Watson. *Contouring: A Guide To The Analysis And Display Of Spatial Data*. Pergamon Press, 1992.

[34] S. Wolfram. *The Mathematica. Fourth edition.* Wolfram Media, 1999.